Microstructured $CH_3NH_3PbI_3$ films for Efficient Solar Cells under Ambient Conditions

Pronoy Nandi [1,2,*], *Chandan Giri* [1], *and D. Topwal* [1,2]

[1]*Institute of Physics, Sachivalaya Marg, Bhubaneswar 751005, Odisha, India*
[2]*Homi Bhabha National Institute, Training School Complex, Anushakti Nagar, Mumbai 400085, India*

Email: pronoy@iopb.res.in; pnphys@gmail.com

Abstract

We demonstrate antisolvent vapor assisted diffusion as a unique technique for controlled nucleation and better crystallization of methylammonium lead iodide, perovskite absorber film for solar cell applications. Our observations also suggest that due to non-covalent weak interaction between the perovskite absorber and the high boiling point antisolvent, Ethylacetate (EA), a new microstructured morphology (micro-rods) evolves in the film, which we report for the first time. It is believed that the changed morphology of the mesoporous films for the high boiling point antisolvent, exhibits better fill factor and results in 32% enhancement of power conversion efficiency than the low boiling point antisolvent, Dichloromethane (DCM), diffused and as-deposited films, thereby suggesting one more parameter to achieve better device performance.

Keywords: *Organic-inorganic hybrid perovskite, antisolvent, micro rods, power conversion efficiency (PCE).*

1. Introduction

Solar cells based on organic-inorganic hybrid perovskite materials, such as $MAPbX_3$ (MA= CH_3NH_3), $FAPbX_3$ (FA= $CH(NH_2)_2$) and mixed (MA, FA, Cs) PbX_3 (X=I, Br, Cl) have sprung to prominence in recent years, due to their remarkable improvements of photovoltaic power conversion efficiencies (PCEs) over the last few years [1-4]. The best photovoltaic devices have already exceeded 22% PCE at the laboratory scale and 15% at the large scale (>1cm^2) [1]. Easy and cost-effective fabrication, strong absorption coefficients, long diffusion length, high charge-carrier mobilities, and apparent defect tolerance makes these devices suitable alternatives to the crystalline silicon and thin-film solar cells [4]. However, abnormal hysteresis, poor long-term stability in air and light, high lead toxicity, and surface/interface issues prevent their entry into the photovoltaic device market [4-6]. The key to improve PCE of hybrid perovskite solar cell is to optimize the morphology of perovskite layer as light absorption, charge transport, and carrier recombination depend on film morphology [1-9]. Thus different fabrication methods like one-step spin coating, two-step sequential deposition, evaporation, vapor, and additive assisted deposition, spray pyrolysis, doctor blade method *etc.* were developed. Recently it was observed that antisolvent method became popular to optimize morphology and improve PCE of hybrid perovskite solar cells [8-14].

Toluene, [11] diethyl ether, [12] chlorobenzene, [7] dichloromethane (DCM) [13] and chloroform [13] have been used in the past as antisolvent to enhance the crystallization of hybrid perovskites. As an example, Jeon *et al.* [11] and Ahn *et al.* [12] improved the crystallization of perovskite films by drip-casting toluene and diethyl ether during the spin-coating process, respectively. However, this technique is not suitable to obtain uniform morphology for large scale devices because dripping antisolvent at the center of the film during spin-coating results in the radial gradient morphology of perovskite films. Later, Zhou *et al.* [14] immersed the large area (1.2 cm^2) spin-coated films in diethyl ether to obtain uniform morphology and achieved PCE as high as 15.3%. However, dipping of perovskite films in anti-solvent might create non-stoichiometry in the sample [14]. To overcome this shortcoming, we develop an antisolvent vapor assisted crystallization (AVC) method for the controlled nucleation and crystallization of hybrid organic-inorganic perovskite thin-films. The key steps of this process are: (a) spin-coated films were kept in an antisolvent environment; but not immersed in the antisolvents and (b) use of low (DCM) and high (EA) boiling point antisolvents. In this study, we show that the choice of antisolvent (depending on their boiling point) plays a significant role in controlling the morphology of perovskite films. Microrods of diameter 1μm were formed when spin-coated films were kept in EA environment; while no microrod formation was observed when DCM was used. X-ray diffraction and energy-dispersive X-ray spectrometry (EDS) measurements confirmed phase purity of the sample; while UV-visible absorption studies, photoluminescence, and X-ray photoelectron spectroscopy were used to characterize the optical and electronic properties of the film and helped us to draw the schematic energy level diagram for the absorber material. In as-deposited and DCM treated films PCE of 5.3% and 5.4% respectively was obtained under atmospheric conditions with >85% humidity. However, 32% of PCE enhancement was observed for 'EA treated mesoscopic films' (7.7%).

2. Experimental Details

a. Material and Sample preparation

The preparation of the precursor solution and light absorber thin films is discussed in this section. 14 mL methylammonium (CH_3NH_2, 40wt% in methanol) was reacted with 15 mL of hydroiodic acid (HI, 57 wt% in water) and the mixture was stirred for two hours under nitrogen atmosphere in an ice bath. The resulting solution was evaporated using a rotary evaporator until white microcrystals of MAI were obtained. These microcrystals were washed in ethyl acetate and were dried at 60^0 C in a vacuum oven overnight and were kept in a vacuum for further use. $MAPbI_3$ precursor solution was prepared by dissolving 691.5 mg of PbI_2 (99.9%, Sigma Aldrich) and 238.6 mg of MAI in 1.5 ml of dimethylformamide (DMF). The resulting solution was spin-coated on FTO glass at 2500 rpm. Upon completion, solvent engineering was performed by transferring the films to EA and DCM environment immediately (except for as-deposited film) and films were dried by heating it at 80^0C for 15 minutes at ambient condition with 85.6% humidity.

b. Solar-Cell device fabrication

Prior to device fabrication, transparent conducting substrate; fluorine-doped tin oxide (FTO) (7 Ω/cm^2) was cut into 1.5 X 1.5 cm^2 pieces and was cleaned by sequential sonication in soap solution, millipore water, isopropanol, followed by drying in Ar flow and plasma treatment for 30 minutes. A compact hole-blocking layer (HBL) of TiO_2 was applied to the clean FTO substrate by the spin-coating at 5000 rpm in air followed by annealing at 500^0C for 30 minutes. The solution required for forming HBL was prepared by mixing Titanium (IV) isopropoxide (2 ml) with 2-methoxy ethanol (10 ml) and ethanolamine (1ml) and heating it to 80^0C for 2 hours under continuous stirring. On top of HBL, a mesoporous layer of TiO_2 was deposited by

spin-coating at 5000 rpm using commercially obtained TiO_2 paste diluted in ethanol (2:7 weight ratio) and annealed at 500^0C for 30 minutes. After cooling to room temperature, perovskite film was deposited on top of mesoporous TiO_2 as discussed in the last section. Further, layer of hole transport material (HTM) (84 mg Spiro-MeOTAD in 1ml chlorobenzene, mixed with 15 µL of 170 mg/ml bis (trifluoromethane) sulfonamide lithium salt dissolved in acetonitrile and 7 µL of tert-butyl pyridine) was grown by spin-coating at 2000 rpm. To complete device fabrication, 100 nm gold contacts were deposited on the top of hole transport layer by thermal evaporation using a shadow mask inside a vacuum chamber with base pressure of 10^{-6} torr.

c. Characterization Techniques

The morphology of as-prepared and antisolvent treated perovskite films was studied by field emission scanning electron microscope (FESEM; Carl Zeiss, Germany), while crystallographic properties of perovskite film on FTO substrate was characterized by XRD (Bruker, D8-advance) equipped with Cu-K_α radiation under the Bragg-Brentano geometry. The optical absorption spectra were measured using an ultraviolet-visible-near-infrared (UV-Vis-NIR) spectrophotometer (Shimadzu, 3101PC) in the wavelength range of 400-800 nm and photoluminescence (PL) emission spectra were acquired using FL920 spectrometer from Edinburg instruments with the excitation energy of 325 nm. I-V measurements of the device were performed using a Newport solar simulator connected to the Keithley 2420 I−V measurement system.

3. Results and Discussion

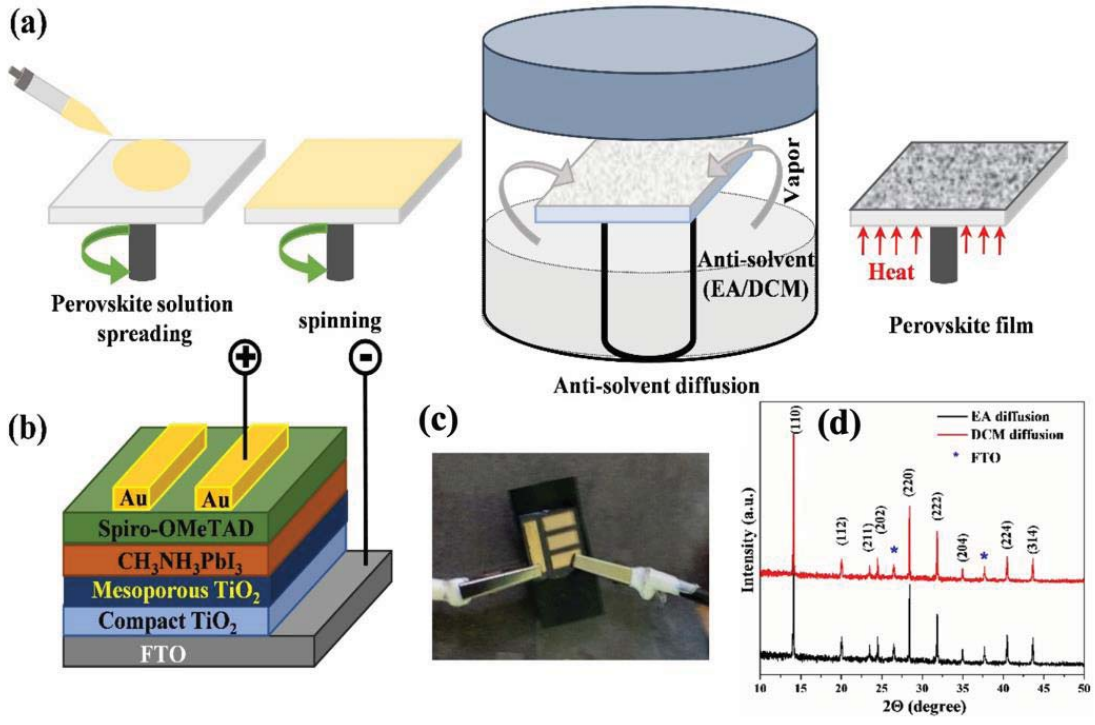

FIG 1. (a) Schematic diagram of the perovskite absorber deposition process using antisolvent vapor diffusion technique. (b) Schematic diagram of the cell architecture. (c) Representative figure of solar cell made by us. (d) XRD patterns of the perovskite films diffused by EA and DCM antisolvents.

Figure 1(a) represents schematics of the process for obtaining $MAPbI_3$ a light absorber layer by anti-solvent vapor assisted crystallization method. The solar cell architecture consists of multilayer films of FTO/compact TiO_2 (HBL)/ Mesoporous TiO_2/ $MAPbI_3$/ Spiro-OMeTAD/ Au. Upon illumination, charge carriers *i.e.*, electrons and holes are generated in $MAPbI_3$. Electrons are transported to the external circuit through TiO_2 as the separation between bottom of the conduction band of TiO_2 and $MAPbI_3$ is very small. Similarly, holes are transported out through the Au electrode via Spiro-OMeTAD as their top of the valence band matches and solar cell current was detected under reverse bias condition. In this architecture, formation of a porous absorber layer is extremely important, and we develop our solvent engineering technology as an effective tool to grow the $MAPbI_3$ layer. This process involves four stages, as depicted in figure 1(a): First, the precursor solution is spread over the FTO substrate; second, spin-coater is accelerated to the desired rotational speed to spread the solution; third, spin-coated film is kept in anti-solvent (EA/DCM) environment (not immersed); finally, the perovskite film is annealed to 80^0 C (see experimental section for details).

It is apparent from figure 2(a-c), the morphology of $MAPbI_3$ thin film has remarkably changed by this solvent engineering process. Figure 2(a) shows the top view of FESEM images of the as-deposited $MAPbI_3$ thin film on FTO glass. Notably, diffusion of DCM anti-solvent had very less effect on the film morphology and structure (Figure 2(b)). In contrast, the difference between as-deposited/DCM diffused film and EA diffused film (Figure 2(c)) is evident. The conventional one-step solution deposition without any antisolvent or with low boiling point antisolvent (DCM; 37^0C) treatment induces typical branchlike crystals, and the FTO surface is not fully covered as confirmed by EDS spectrum (Figure 2(d)). Whereas, micro rods of diameter 1μm were formed when spin-coated films were kept in the EA environment, Figure 2(c), with better coverage. This improved morphology of mesoporous film by the high boiling point antisolvent (EA; 77^0C) is ascribed to the non-covalent weak interaction between the precursor solvent and antisolvent. During the process of nucleation and crystallization, DCM evaporates quickly as soon as it interacts with the film (as boiling point is low) and has no profound effect on its morphology; whereas EA can assist crystallization by exploiting non-covalent weak interaction (due to high boiling point) and in the process microstructures are formed. In order to study the local chemical composition and to accesses the relative differences in the elemental compositions in DCM and EA diffused films, EDS analysis was performed and data is depicted in figure 2(d). EDS elemental mapping on figure 2(b) and 2(c) are presented in figure 2(d) and the results confirmed that EA diffused film has more coverage than that of DCM diffused film and the ratio Pb:I is close to the actual composition (1:3) for EA treated film, whereas in the DCM treated film the ratio is 1:2.7. Incomplete conversion of the precursor in the synthesis process for the case of DCM diffused film might be responsible for this iodine deficiency [15-16].

To identify the phase purity of both the samples (DCM and EA-treated films) and to get more information about the structure, XRD was performed and is presented in figure 1(d). Observation of sharp well-defined peaks confirms the crystalline nature of the perovskite films, it crystallizes in the tetragonal phase (I*4/mcm*) [2-3]. Diffraction peaks appearing at 26.49^0 and 37.67^0, marked by asterisks in figure 1(d) arise from the underlying FTO substrate and peaks at 14.11^0 and 28.44^0 correspond to the (110) and (220) crystal planes of the perovskite film. Further, optical studies (UV-Visible absorption) of micro-structured thin film (EA treated $MAPbI_3$) was performed to find its potential as absorber material in solar cell. The UV-Visible absorption spectrum of EA treated $MAPbI_3$ reveals strong absorption in the visible region with an absorption edge at 771 nm (figure 3(a)), which can be attributed to band-to-band direct transition and is consistent with previous reports [2-3,17]. XPS valence band (VB) spectrum acquired from this sample is depicted in figure 3(b), where the main feature (2-6 eV) arises due to nonbonding I 5*p* orbitals, along with a dominant contribution from antibonding Pb 6*s*, as observed from band structure calculations [17-18]. Linear

interpolation of VB spectra and its intersection with the baseline as shown in figure 3(b), it gives the energy of the top of the valence band, further using the absorption spectrum separation between VB and CB can be extracted and schematic energy level diagram is drawn in Figure 3(c), where energies of top of the VB, bottom of CB is presented with respect to E_F, which is denoted as 0 eV. A proper understanding of this energy level diagram of hybrid perovskite is essential to identify the appropriate electron and hole transport materials for the efficient fabrication of solar cell devices.

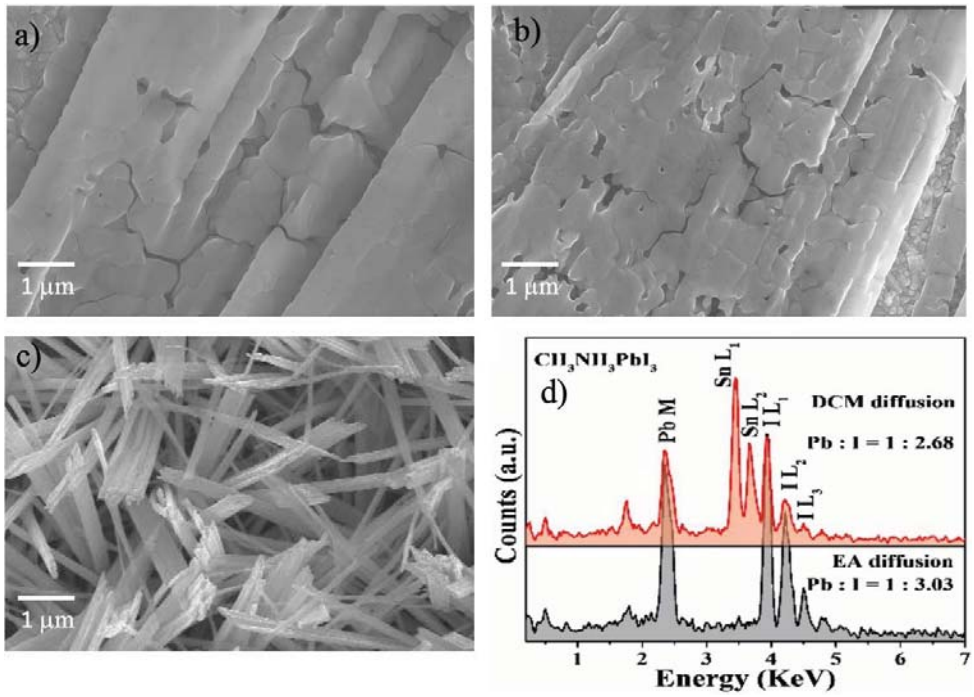

FIG 2. SEM images of the perovskite films (a) as-deposited, (b) DCM-diffused, (c) EA diffused. (d) EDS of the perovskite films diffused by EA and DCM antisolvents.

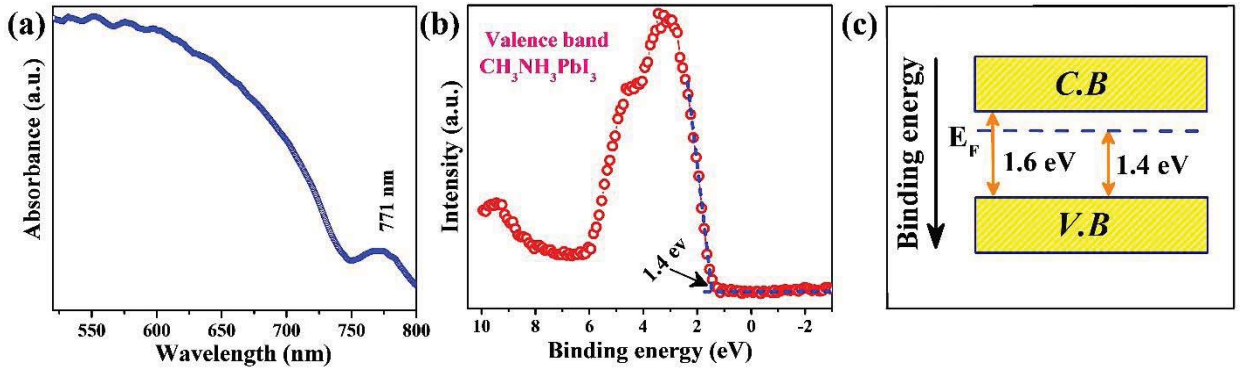

FIG 3. (a) UV-visible absorption spectra and (b) Valence band XPS spectra of EA diffused $CH_3NH_3PbI_3$ thin film. (c) Schematics of the energy level diagram for EA diffused $CH_3NH_3PbI_3$ film.

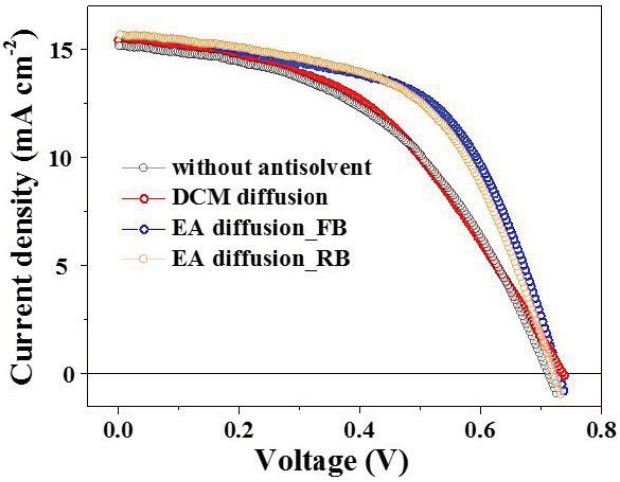

FIG 4. Effects of antisolvents (DCM and EA) on the photovoltaic device performance in an ambient atmosphere.

Photovoltaic performance of the perovskite solar cells with a structure of FTO/compact TiO_2 (HBL)/Mesoporous TiO_2 (ETL) /$MAPbI_3$/Spiro-OMeTAD (HTL)/Au was measured under AM1.5 simulated solar illumination (100mW/cm^2). Blue and orange open circles in Figure 4 presents the J–V curves for a cell fabricated by high boiling point antisolvent diffusion, measured with a 40 ms scanning delay in reverse (from the open-circuit voltage (V_{oc}) to the short-circuit current (I_{sc})) and forward (that is, from I_{sc} to V_{oc}) modes under standard airmass 1.5 global (AM 1.5 G) illumination, whereas gray and red circles in Figure 4 denotes the forward bias J-V curves for as-deposited and low boiling point antisolvent diffused solar cells. Table 1 summarizes the extracted short-circuit current density (J_{sc}), open-circuit voltage (V_{oc}), and fill factor (FF). Perovskite solar cell prepared by high boiling point antisolvent diffusion exhibits the highest power conversion efficiency (PCE) of 7.7% with negligible hysteresis. These films show the formation of micro rods, suggesting that morphology plays an important role. A comparative study on current density vs. voltage plots of all three samples is depicted in figure 4 and the summary of device performance is presented in Table-1.

Table 1. Summary of Solar Cell Device Performance (in ambient conditions)

Sample synthesis process	Current density (mA/cm^2)	Open-circuit Voltage (Volt)	Fill-factor (%)	PCE (%)
As deposited Film (without anti-solvent)	15.15	0.72	51.44	5.6
DCM diffusion	15.43	0.73	51.80	5.8
EA diffusion (Forward Bias)	15.53	0.74	66.13	7.7
EA diffusion (Reverse Bias)	15.52	0.73	67.33	7.6

Table-1 demonstrates that the devices made of without antisolvent or low boiling point (DCM) antisolvent diffused perovskite active layer results poor device performance than high boiling point (EA) antisolvent diffused active layer. As seen from Table-1, devices made by the above three methods yielded almost same J_{sc} and V_{oc}, however, due to the enhancement of fill-factor(FF) for EA diffused film, efficiency enhanced. As seen from SEM images in figure 3, the formation of perovskite micro rods enhances the sample coverage in

the film and prevents electric shunting between the electrodes, and markedly enhanced the FF of the device. Thus, high device performance is attributed to the formation of micro rods due to the weak interaction between hybrid perovskite and the high boiling point antisolvent (EA).

4. Conclusion

In summary, we developed an antisolvent vapor assisted crystallization technique for the deposition of perovskite layer and demonstrated a solution-processed mesoporous perovskite solar cell with 7.7% PCE under standard conditions (AM 1.5 G radiation,100 mW cm^{-2}) in atmospheric conditions with >85% humidity. We also demonstrated a plausible mechanism for the formation of new morphology (micro rods) of perovskite layers during the solvent-engineering process. Due to non-covalent weak interaction between the perovskite absorber and the high boiling point antisolvent (EA), micro rods were grown via an intercalation process. UV-visible absorption and XPS studies were performed to characterize the optical and electronic properties of EA treated film and a schematic energy level diagram of the perovskite material is presented. Further, we also observed that EA-treated perovskite solar cell exhibits a power conversion efficiency of 7.7%, which is 32% higher than that of DCM treated (5.8%) and without antisolvent diffused (5.6%) solar cells. This insight will open the possibility of preparing organic-inorganic lead halide perovskite-based materials with phase stability in ambient conditions to improve the performances of optoelectronic devices.

5. Acknowledgments

The authors thank Prof P.V.Satyam (IOP, BBSR) and Dr. P. Guha for their support in carrying out FESEM measurements. The authors would also like to acknowledge Prof. S. C. Ogale (IISER, Pune) and U. Bansode for their help in carrying out I-V measurements.

REFERENCES

[1] J. Huang, Y. Yuan, Y. Shao, Y. Yan, Nature Reviews Materials, 2, 17042 (2017).

[2] P. Nandi, C. Giri, U. Bansode, D. Topwal, AIP Conference Proceedings, 1832, 080065 (2017).

[3] P. Nandi, C. Giri, B. Joseph, S. Rath, U. Manju, D. Topwal, J. Phys. Chem. A, 120, 9732-9739 (2016).

[4] G. E. Eperon, M. T. Horantner, H. J. Snaith, Nature Reviews Chemistry, 1, 0095 (2017).

[5] P. Nandi, C. Giri, D. Swain, U. Manju, S. D. Mahanti, D. Topwal, ACS Appl. Energy Mater., 1, 3807–3814 (2018).

[6] Q. Zhang, F. Hao, J. Li, Y. Zhou, Y. Wei, H. Lin, Science and Technology of Advanced Materials, 19, 425-442, (2018).

[7] M. Xiao, F. Huang, W. Huang, Y. Dkhissi, Y. Zhu, J. Etheridge, A. Gray-Weale, U. Bach, Y. B. Cheng, L. Spiccia, Angewandte Chemie, 126, 10056-10061 (2014).

[8] J. Li, R. Yang, L. Que, Y. Wang, F. Wang, J. Wu, S. Li, J. Mater. Res., 34, 2416 (2019).

[9] K.-M. Lee, C.-J. Lin, B.-Y. Liou, S.-M. Yu, C.-C. Hsu, V. Suryanarayanan, Organic Electronics, 65, 266-274 (2019).

[10] H. Zhou, Q. Chen, G. Li, S. Luo, T.-b. Song, H. S. Duan, Z. Hong, J. You, Y. Liu, Y. Yang. Science, 345, 542-546 (2014).

[11] N. J. Jeon, J. H. Noh, Y. C. Kim, W. S. Yang, S. Ryu, S. II Seok, Nat. Mater., 13, 897-903 (2014).

[12] N. Ahn, D. Y. Son, I. H. Jang, S. M. Kang, M. Choi, N.-G. Park, J. Am. Chem. Soc., 137, 8696-8699 (2015).

[13] Y. C. Choi, S. W. Lee, D.-H. Kim, APL Mater. 5, 026101 (2017).

[14] Y. Zhou, M. Yang, W. Wu, A. L. Vasiliev, K. Zhu, N. P. Padture, J. Mater. Chem. A, 3, 8178-8184 (2015).

[15] G. F. Samu, A. Balog, F. De Angelis, D. Meggiolaro, P. V. Kamat, C. Janaky, J. Am. Chem. Soc., 141, 10812-10820 (2019).

[16] D. Meggiolaro, S. Motti, E. Mosconi, A. Barker, J. Ball, C. A. R. Perini, F. Deschler, A. Petrozza, F. De Angelis, Energy Environ. Sci. 11, 702–713 (2018).

[17] P. Nandi, C. Giri, U. Manju, D. Topwal, CrystEngComm, 21, 656-661 (2019).

[18] P. Nandi, S. K. Pandey, C. Giri, V. Singh, L. Petaccia, U. Manju, S. D. Mahanti, D. Topwal, J.Phys.Chem.Lett. 11, 5719-5727 (2020).